Renewable Energy 237 (2024) 121545

Contents lists available at ScienceDirect

Renewable Energy

journal homepage: www.elsevier.com/locate/renene

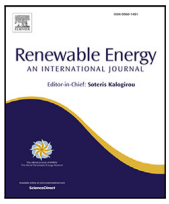

Microalgae bio-reactive façade: A model coupling weather, illumination, temperature, and cell growth over the year

Victor Pozzobon

Université Paris-Saclay, CentraleSupélec, Laboratoire de Génie des Procédés et Matériaux, Centre Européen de Biotechnologie et de Bioéconomie (CEBB), 3 rue des Rouges Terres 51110 Pomacle, France

ARTICLE INFO

Dataset link: https://github.com/victorpozzobon/biofacade

Keywords:
Microalgae
Biofaçade
Production
Biological model
Temperature

ABSTRACT

This article presents the development of a numerical model coupling the thermal and biological behaviors of a microalgae biofaçade. Heat fluxes and illumination are modulated by actual weather data, and the system response is evaluated in terms of biomass and pigment production. First, the effect of the different model refinements are screened. Then, the model is applied to an illustrative case: the city of Marseille over the year 2023. The results illustrate the model's capabilities, such as assessing the building/biofaçade thermal synergy or the summer/winter operational differences. The numerical behavior of the model is also analyzed: local and global sensitivity analyses assess the impact of uncertain parameters. The parameter inducing the highest amount of uncertainty is the microalgae photoconversion efficiency, highlighting the need to ascertain its value before designing a system. Despite this uncertainty, even under conservative assumptions, the predictions of the model are 10 % accurate.

1. Introduction

During the last century, there has been a significant increase in the human population and notable enhancements in the quality of life. However, these developments have placed considerable strain on our ecosystem. As indicators of this pressure, one could name the depletion of fossil fuels, water scarcity, loss of arable lands, and biodiversity decline [1]. In response to this pressing situation, microalgae have emerged as a potential solution to help humanity mitigate its environmental impact. Microalgae possess the ability to produce valuable molecules of interest to various sectors, from food and feed (proteins, vitamins, ...) to cosmetics and pharmaceuticals (texturizers, antioxidants, ...) [2,3]. Moreover, their cultivation offers ecological benefits such as CO_2 fixation [4], phosphate fixation [5], nitrogen fixation [6], or effluent bioremediation [7]. Despite their potential, numerous scientific challenges must be addressed before microalgae can fully deliver on their promises. Among them, reducing the cost of microalgae production is key.

As for any process, upscaling the production system offers perspectives of cost reduction. In the case of microalgal biotechnology, this means opting for outdoor cultivation to access large and free amounts of the limiting resource, which is light. However, at least two drawbacks are to be anticipated. First, large pieces of land would have to be acquired. Second, even in closed photobioreactors, the culture would be submitted to natural cycles when it comes to light and temperature. These cycles represent a challenge in terms of bioprocess control, especially the temperature one. Indeed, too low temperatures prevent the microalgae from optimally using the available light (*e.g.*, a bright day in winter) and, even worse, the too hot temperatures can harm the cells (irreversible denaturation of proteins and DNA [8]) and lead to culture loss.

Acknowledging these limitations, an idea has sparked: integrating microalgae photobioreactors into building façades. These façade-integrated microalgae photobioreactors (in short bio-reactive façades or biofaçades) represent a promising synergy between a building and a biological system and have been acknowledged as belonging to the group of the high-performance architectures technological solutions [9,10]. Mutual benefits are envisioned. One the photobioreactors side, integrating them into buildings could help mitigate expenses by offering vertical support, utilities (*e.g.*, water, thermal regulation), and potentially nutrients (*e.g.*, carbon dioxide reclaimed from the building). On the building side, numerous advantages are anticipated. Integration of photobioreactors could provide shading, enhance thermal comfort by better modulating incident heat compared to traditional glazing during summer, lower induced pollution, generate revenue streams, and contribute to aesthetic enhancements.

Despite the great promises of this technology, to date, only a few studies can be found in the literature. The most basic ones are experiments on a microalgae biofaçade module alone (isolated from a potential host building) [11–13]. While simple, they delivered insights on the relevance of some design choices (*e.g.*, using PolyMethyl

E-mail address: victor.pozzobon@centralesupelec.fr.

https://doi.org/10.1016/j.renene.2024.121545
Received 26 May 2024; Received in revised form 2 October 2024; Accepted 5 October 2024
Available online 16 October 2024

MethAcrylate, PMMA in short, instead of glass to reduce the building static load), or key figures, such as an optimal productivity of 10.5 g/m^2/day for *Chlorella vulgaris*. They also highlighted the trade-off between a narrow light path, fostering high-density microalgae culture, and the system U-value that may not favor building insulation. Finally, they acknowledged that thermal integration with the building was pivotal in improving the system's performance.

In addition to experimental investigation, numerical modeling initiatives have been undergone. Classical approaches such as mass and heat balances (convective-radiative), sometimes coupled with Computational Fluid Dynamics or actual weather data, have been applied to investigate various scenarii, such as double-skin façade [14–17] or direct integration as glazing [18,19]. Among them, the work led by Pruvost's team is of note as it might be the only coupling experiments and numerics. While theoretical, these investigations confirmed the relevance of the envisioned synergy between the host building and the biofaçade. To name a few, the biofaçade sizably limits the need for cooling during summertime and moderately reduces the requirement for heating during wintertime [17]. In addition, the host building effectively warms the culture during wintertime, mitigating the seasonability effect an outdoor system could be confronted with. While, in summertime, it offers a heat sink, avoiding lethal overheating [18]. Still, the versatility of the different numerical tools deployed for those investigations allowed to expand the scope beyond the sole microalgae production and thermal integration, and tackle the question of occupant comfort. For example, Sarmadi et al. conducted a numerical investigation into the visual comfort aspects associated with microalgae biofaçade integration [20]. The study focused on a contemporary office building with a mezzanine (located in Tehran, for their study). Visual comfort entails balancing sunlight availability with the risk of potentially blinding glare. The researchers concluded that microalgae biofaçades effectively mitigate the occurrence and intensity of blinding glare in sunny environments. However, to prevent excessively dark configurations, they needed to be combined with conventional double-glazing. Furthermore, to enhance the aesthetic refinement of the technology, it is conceivable to partition the biofaçade into multiple culture compartments, each housing microalgal species of varying colors [21].

Finally, one of the most significant studies worth mentioning involves the implementation of 185 m^2 of biofaçade in the BIQ house located in Hamburg, Germany, [22]. This field trial marked a substantial advancement for the technology. The biofaçades were affixed as a double skin to the building structure. These modules, standing at 2.5 m in height, comprised glass with an 18 mm cultivation compartment and an air layer, branded as *SolarLeaf*. Throughout the year 2014, the system achieved a solar-to-biomass conversion efficiency of 4.4%, which is comparable to laboratory studies on microalgae photoconversion efficiency (*e.g.*, 5.01% [23], 5.65% [24], or 4.34% [25]), along with a 21% thermal energy recovery efficiency. Additionally, the trials underscored the critical influence of temperature on the growth of *Chlorella vulgaris*. Beyond technical aspects, this field deployment also highlighted the notably positive social acceptance of the technology.

All the studies above have helped the technology grow from a mere idea to a solid concept worth being challenged in the field. Yet, the road is still long before biofaçades cover megalopolis buildings. Together, scholars and engineers have tackled biofaçade design (material, geometry, ...) [11–13,18], integration (glazing or double skin) [14,15,18], location dependence [17], and thermal synergy with the host building [16]. Among the steps along the path towards large-scale deployment, biological performance assessment is the next in line. Indeed, while of interest, thermal synergy is only one side of the benefits offered by a microalgae biofaçade. Biological production is the other. Its evaluation will unravel CO_2 biofixation capabilities, the potentiality for cleaning the building's gaseous and liquid streams, and revenue generation estimation. However, like thermal performances, biological performances are subjected to circadian and seasonal cycles and weather modulations. Considering the complexity at hand, numerical modeling is the best option before opting for large-scale, long-running, and expensive trials. Therefore, this article aims to provide scientists and technicians with a tool capable of coupling location, module design, weather conditions, and microalgal strain biological behavior to predict the biotechnological performances of a given implantation.

To do so, the proposed model builds on top of a previous one, focusing on the thermal aspects [18,19]. In a nutshell, to predict the microalgae culture temperature, the previous model accounts for direct incident illumination from the sun, radiative heat exchange with the sky, radiative heat exchange with the surrounding (buildings, fields,...,depending on the location), convective heat exchange with the outdoor air, radiative and convective exchange with the building hosting the biofaçade, and heat supplied and removed by the gas flow sparging within the culture medium. All these phenomena are modulated by location (sun path model), the weather (almost 30 years of data from the French weather forecast agency), and the design of the biofaçade (*e.g.*, single or double glazing, radiation-selective film, reservoir thickness, ...). While detailed, the former model predicted adequate operational time for microalgae production, which is defined as temperature neither too cold nor too hot and sufficient illumination. Still, it does not predict microalgae biomass production itself (in terms of mass per unit of time) or its quality.

Consequently, the present article will take it to the next stage by adding a biological model predicting the growth of *Chlorella vulgaris* and its pigment content (a proxy of biomass quality). *Chlorella vulgaris* was chosen as the model strain as it is commonly encountered in both industrial and scientific communities, approved as food and feed by (European Food Safety Authority - Ares (2022) 1668627 - and US Food and Drug Administration - GRN 00396 -), and features a sizable biotechnological potential [26]. Furthermore, recent studies have provided insight into cell growth under varying light [27,28] and temperature [29], which allow faithful modeling its performances. Here, the focus will be set on the elaboration of the model and its refinements (how to account for cell maintenance, level of accuracy in the description of the light/microalgae interaction, ...). As this conceptual and numerical work represents a sizable amount in itself, its application to bioprocess design, control, and optimization is presented in a companion article.

2. System & models

2.1. Considered system

Fig. 1 introduces a schematic overview of the microalgae biofaçade under consideration, along with potential design variations. Additionally, the graphical abstract illustrates the integration of a biofaçade model into its environment. At the heart of the system lies a reservoir containing the microalgae culture. This reservoir is enclosed by two layers of PMMA and incorporates gas spargers at the base and a vent at the top. The standard dimensions of the system are 1 m in width and 4 m in height, mirroring typical office building floor heights. The thickness of the system varies based on design decisions. Moreover, the biofaçade is envisioned to be integrated into an office building façade at a height of approximately 20 m above ground level to optimize sunlight exposure (in the opposite case, the reader is kindly referred to Elmalkly et al. work who addressed the question of modules submitted to overcast shadows [30]). Finally, it is considered positioned centrally on the façade, as it facilitates taking into account outdoor convective heat transfer induced by wind [31].

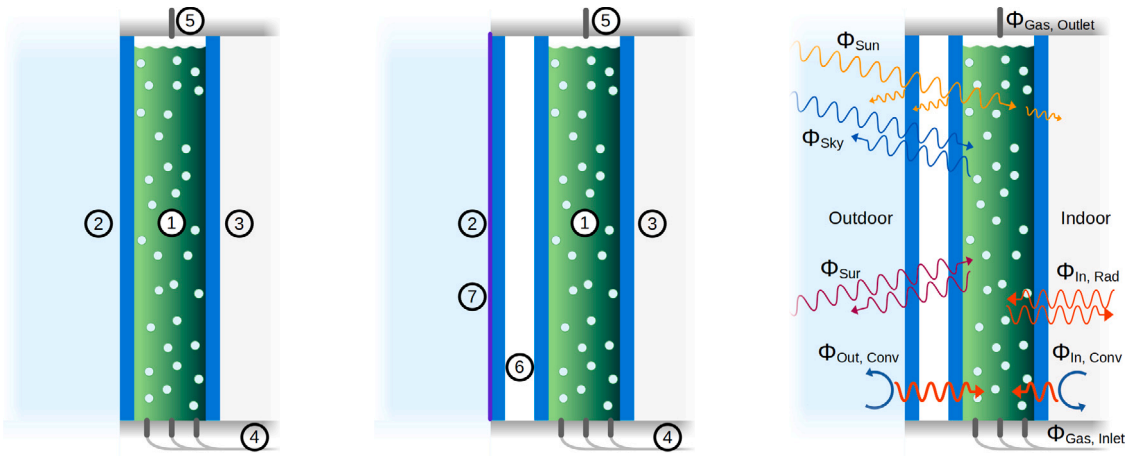

(a) Basic design (b) Double glazing & radiation selective film design (c) With heat fluxes

Fig. 1. Schematic representation of possible microalgae biofaçade designs. 1 - microalgae culture reservoir, 2 - outward PMMA layer, 3 - inward PMMA layer, 4 - gas sparging system, 5 - vent, 6 - double glazing, 7 - radiation-selective film. The reported heat fluxes (Φ) are introduced in the text.

2.2. Assumptions and model classification

From a conceptual point of view, microalgae growth in outdoor or hybrid photobioreactors, such as a microalgae biofaçade, can be considered depending mainly upon two physical parameters: absorbed light and temperature. Absorbed light supplies the cells with the energy required to power their proliferation while temperature modulates their metabolic rates. On the one hand, only accounting for these two parameters is a dramatic simplification of the system, as one neglects considerations on the quality of mixing within the culture compartment (assuming perfect mixing), on pH (assumed adequate), on nutrient supply (assumed sufficient and not inhibitory), and potentially aggressive bacterial contamination (assumed absent), among others. On the other hand, it represents a quite complex challenge already. Indeed, accurately accounting for them already requires dealing with numerous refinements, as will be detailed in the coming sections.

Still, before diving into the model elaboration, it is worth taking a step back and contextualizing it with respect to other scholars' works. Photobioreactor models like the one foreseen can be classified into three types depending on how they account for microalgae light interaction. In their work, Bechet et al. discriminated them as type I - based on external illumination -, type II - based on internal illumination distribution -, and type III - accounting for cell motion within the light field [32]-. The proposed model belongs to the second category. Then comes the question of how light power is used to drive cell proliferation. Two different approaches can be noted to tackle this question. The first one could be called "light-activated Monod law", as growth is defined by a growth rate, so long the illumination is adequate, cells proliferate with no regard towards an energy balance. This is, for example, the case of Esposito et al.'s model [33]. The second category could be called "light balance-based models". In this approach, actual cell light absorption is used to account for an energy balance. Therefore, even though light is adequate, growth is still limited by the captured amount of light energy. This is, for example, the case of Hoeniges et al.'s model [34]. The second category could be deemed closer to reality. This is why the proposed model was built on this paradigm.

2.3. Thermal model

The thermal behavior model of the biofaçade is detailed, validated, and thoroughly analyzed in two companion articles [18,19], with a summary provided in the Supplementary Materials. In essence, the model calculates the evolution of the microalgae reservoir temperature by summing the contributions of absorbed and emitted convective-radiative heat fluxes (Fig. 1 - right). The considered heat fluxes include:

- incident direct sunlight, Φ_{Sun} which is divided into visible and infrared radiation,
- incident and emitted radiation towards the sky, Φ_{Sky},
- incident and emitted radiation towards the surroundings, Φ_{Sur},
- incident and emitted radiation towards the host building indoor, $\Phi_{In,Rad}$,
- convective-conductive exchange with the outdoor air, $\Phi_{Out,Conv}$,
- convective-conductive exchange with the indoor air, $\Phi_{In,Conv}$,
- heat inflow from the sparged gas, $\Phi_{Gas,Inlet}$, and heat outflow from the vented gas, $\Phi_{Gas,Outlet}$.

Conductive heat fluxes within the PMMA and stagnant air layers are described using a resistance in series model. Convective exchanges are modeled based on correlations derived from experimental data. Additionally, solar illumination is described using the model proposed by the Illuminating Engineering Society, which considers solar time, Earth position, cloud cover, and orientation [35]. Radiative exchanges with the surroundings, given limited information, are modeled using the Stefan–Boltzmann formula weighted by relevant view factors and emissivities.

2.4. Weather data and timescales

Meteorological data driving the model were sourced from Météo-France, the public French weather forecast agency, covering France with approximately one station per administrative region. Data range from 1996 to the present, with measurements taken every three hours. Key parameters utilized in this study include air temperature, cloud cover, wind velocity (at 10 m above the ground), wind direction, relative humidity, and static pressure. The database was last accessed in March 2024. Collectively, these model components enable the determination of the illumination the culture receives, as well as, the heat fluxes it exchanges with its surrounding and, therefore, its temperature evolution over time.

In addition to power the model with the description of the weather condition, one should note that the meteorological data dictate the timescale of the model. Indeed, any phenomena having a characteristic time far below this value can be described in a static manner using a steady-state equation (*e.g.*, light profiles within the culture compartment). On the contrary, any phenomenon having a timescale near or above this value has to be described dynamically using differential equations (*e.g.*, microalgal cell proliferation, cell pigment content acclimation, ...).

2.5. Illumination model

From a biological standpoint, incident light has two pivotal effects on the microalgal culture hosted within the reservoir: it supplies the energy required for the culture to grow and modulates the efficiency of its own usage by the cells. It is therefore crucial to model it. From the incident illumination and the biomass optical properties, it is possible to derive the power absorbed by the culture using Beer–Lambert law (Eq. (1)):

$$\Phi_{Abs,Vis} = S\Phi_{Inc,Vis}(1 - exp(-\sigma_{Abs}XL)) = SI_0k(1 - exp(-\sigma_{Abs}XL)) \quad (1)$$

where S is the sun collection surface, $\Phi_{Inc,Vis}$ is the incident power (in W/m^2) within the visible range of the spectrum, given by the solar path model and weather conditions. This parameter can be expressed in μmolPhoton/m^2/s using a conversion factor (k = 2.3495 μmolPhoton/J) specifically established for the sun to yield I_0 is the incident illumination. σ_{Abs} is the light absorption cross of the cells, X the cell concentration, and L the culture reservoir thickness. Furthermore, elements gathered by [27,28] suggest that, in a flat panel photobioreactor, such as biofaçade, microalgae growth is controlled by the averaged illumination in the culture volume ($I_{Average}$). It is therefore mandatory to evaluate this quantity. Luckily, it can easily be obtained by volume-averaging Beer–Lambert law (Eq. (2)).

$$I_{Average} = \frac{I_0}{\sigma_{Abs}XL}(1 - exp(-\sigma_{Abs}XL)) \quad (2)$$

In order to be as faithful as possible, and even though minor, indoor illumination was taken into account. The US Occupational Safety and Health Administration advises 30 foot candle in office environment [36]. Assuming a cold white spectrum for indoor lighting, it can be converted to 4.61 μmolPhoton/m^2/s in the solar spectrum (assumed to be on from 7 am to 9 pm, 5 days a week).

2.6. Biological model

2.6.1. Phototrophic growth model

The biological model used in this work is based on mass and energy balances. Cell mass variation is driven by the transformation of absorbed light power into new biomass and modulated by culture maintenance. Combining these three phenomena yields the main equation of the model, *i.e.*, the one governing the cell proliferation:

$$\underbrace{V\frac{dX}{dt}}_{\text{Cell mass variation}} = \underbrace{\frac{\Phi_{Abs,Vis}(I_0,X)}{HHV}\xi(I_{Average})}_{\text{Absorbed power and usage efficiency}} - \underbrace{VmeX}_{\text{Maintenance}} \quad (3)$$

where V is the culture reservoir volume, HHV the biomass Higher Heating Value, ξ the photoconversion efficiency (a.k.a. photosynthetic efficiency), and me the maintenance rate. As one can see, most of the model complexity relies on how the photoconversion efficiency is expressed. To build a coherent expression of the photoconversion efficiency versus volume-average illumination, several elements will be considered.

First of all, insightful experiments were performed to acquire *Chlorella vulgaris* growth rate under increasing light intensities [28]. These experiments exposed *Chlorella vulgaris*, under optically thin (isoactinic) conditions, to light intensities ranging from 25 to 800 μmolPhoton/m^2/s and reported, among other, acclimated growth rates and pigment contents. From the reported growth rate data, it is possible to model the gross cell growth rate:

$$\mu_{Gross}(I_{Average}) = \mu_{Net}(I_{Average}) + |me| \quad (4)$$

where $\mu_{Net}(I_{Average})$ is derived from the experiments and me known from other dedicated experiments [25]. Based on experimental data, $\mu_{Gross}(I_{Average})$ can be described as a sigmoid function (Eq. (5)) and the associated parameters obtained by a classical fitting procedure (μ_{Max} = 2.17 ± 0.00 1/day and I_{Ref} = 48.3 ±0.5 μmolPhoton/m^2/s, Fig. 2 - left). This description yields a Root Mean Square Error (RMSE) of 0.074 1/day. For the sake of completeness, this law was compared to an arctangent function and Michaelis–Menten function, which achieved higher RMSE values (0.099 and 0.107 1/day, respectively).

$$\mu_{Gross}(I_{Average}) = 2\mu_{Max}\left(\frac{1}{1 + exp(-I_{Average}/I_{Ref})} - \frac{1}{2}\right) \quad (5)$$

Second of all, the photoconversion efficiency in optimal conditions was measured at 4.34% (ξ_0) for *Chlorella vulgaris* by Oliver et al. [25]. To access this data, experiments were carried out in the photolimited zone of the PI curve (Photosynthesis vs. Irradiance, a.k.a. PE curve), which is below 150 μmolPhoton/m^2/s for *Chlorella vulgaris* [37], under nutrient-replete conditions. Under such conditions, the photoconversion efficiency is at its maximum, and the cell growth rate increases linearly as the illumination increases [38]. Still, above a given light intensity, the growth rate plateaus (from 150 μmolPhoton/m^2/s up to 800 μmolPhoton/m^2/s or more [28]) at a fixed value (μ_{Max}). Consequently, the photoconversion efficiency decreases. With these considerations, it is possible to write the photoconversion efficiency as the ratio of the ideal growth rate (as if the linear dependency over illumination was endless) and the actual growth rate:

$$\begin{aligned}\xi(I_{Average}) &= \xi_0\frac{\mu_{Gross}(I_{Average})}{\frac{d\mu_{Gross}}{dI}|_{I=0}I_{Average}} \\ &= \xi_0\frac{4I_r}{I_{Average}}\left(\frac{1}{1 + exp(-I_{Average}/I_{Ref})} - \frac{1}{2}\right)\end{aligned} \quad (6)$$

where the denominator accounts for the linear increase following the initial slope of the PI curve, and the numerator is the observed growth rate. With $\xi(I_{Average})$ modeled, it is, therefore, possible to predict cell mass variation within the biofaçade for a given light volume-averaged light intensity by integrating Eq. (3).

2.6.2. Asymptotic validation

Still, before applying the proposed model, its validity is to be challenged. Let us assume a configuration under which the microalgal culture is diluted and the optical thickness of the system is low. In addition, let us assume that this incident illumination of 200 μmolPhoton/m^2/s (high enough for the culture to be conducted in the photosaturation part of the PI curve, above 150 μmolPhoton/m^2/s). Consequently, $I_{Average} \simeq I_0$, $\Phi_{Abs,Vis}$ can be written as Eq. (7) (first order Taylor expansion of Eq. (1), note the introduction of the k factor to convert μmolPhoton/m^2/s to W/m^2), the photconversion efficiency as in Eq. (8) (as the term $exp(-I_{Average}/I_{Ref})$ of Eq. (6) come close to $exp(-4)$, *i.e*, 0), and the overall balance as Eq. (9).

$$\Phi_{Abs,Vis} = S\frac{I_0}{k}\sigma_{Abs}XL \quad (7)$$

$$\xi(I_0) = \xi_0\frac{2I_{Ref}}{I_0} \quad (8)$$

$$V\frac{dX}{dt} = \frac{SI_0\sigma_{Abs}XL}{kHHV}\xi_0\frac{2I_{Ref}}{I_0} - VmeX = V\frac{2k\sigma_{Abs}\xi_0I_{Ref}}{HHV}X - VmeX \quad (9)$$

Still, in these conditions, one would expect the growth rate to be maximal. It can therefore be written that $\mu_{Max} \simeq \frac{2\sigma_{Abs}\xi_0I_{Ref}}{kHHV}$. Yet, computing the right-hand side of the equation is only possible by knowing the absorption cross section of the cells (σ_{Abs}). Luckily, some authors tackled this difficult question [39,40]. However, directly using their values would void the validity of the parameters formerly identified (ξ_0, I_{Ref}, and μ_{Max}). Therefore, an alternative approach is to be used here: the cross section should be calculated based on the obtained equation and the computed value for σ_{Abs} compared to the ones reported in the literature. In this case, the obtained absorption cross section value is 288 m^2/kg, which is relatively close to the ones reported by Kandilian et al. and Baránková et al. (253 ± 2 m^2/kg

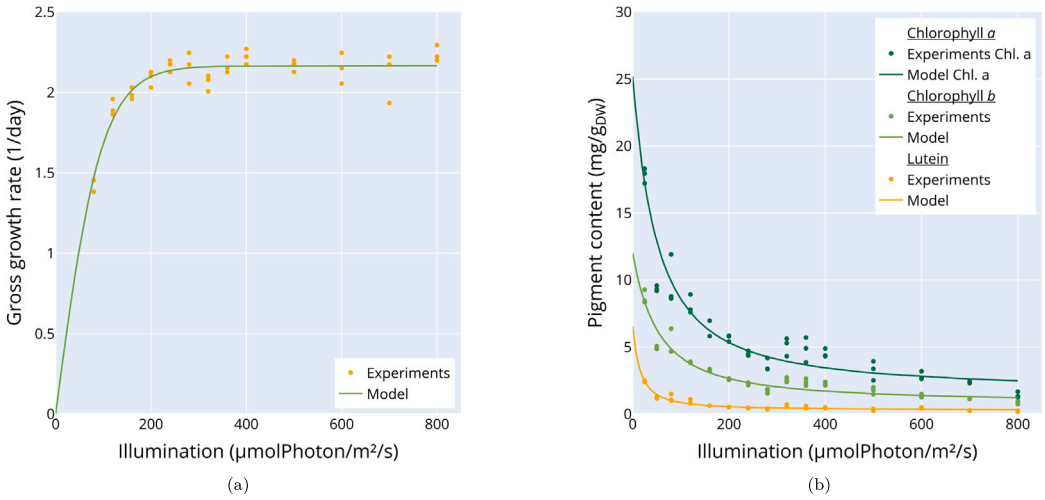

Fig. 2. Experimental data and their numerical reproduction. Left — gross growth rate. Right — cell pigment contents.

Table 1
Parameters describing the cell equilibrium pigment content, with 95% confidence interval.

Pigment	A (mg/g_{DW})	a (–)	b (μmolPhoton/m^2/s)	RMSE (mg/g_{DW})
Chlorophyll *a*	25.2 ± 0.06	0.361 ± 0.001	56.7 ± 0.3	0.949
Chlorophyll *b*	12.0 ± 0.02	0.364 ± 0.000	59.4 ± 0.2	0.625
Lutein	6.53 ± 0.01	0.315 ± 0.000	17.6 ± 0.2	0.318

for the whole visible spectrum by averaging the two studies) [39,40]. Obtaining similar values by such an indirect approach is a token of the model's reliability.

2.6.3. Cell pigment content acclimation

In addition to determining cell proliferation, the proposed numerical tool can also tackle another fundamental question of outdoor microalgae cultivation: their acclimation to the constantly evolving illumination. To describe this behavior, one has to consider two aspects: the equilibrium value of the biomass pigment content for a given illumination and the time cells need to acclimate and reach this value. Like for growth rate, the first aspect was dealt with in detail experimentally, and values specific to *Chlorella vulgaris* could be recovered (Fig. 2 - right). Regarding the time required for cells to reach the equilibrium pigmentation, very few authors tackled this question. Among them, the works of Cullen [41] and De Mooji [42] and their co-authors are to be acknowledged. The first team worked with a diatom species (*Thalassiosira pseudonana* - clone 3H -) to which both low-to-high and high-to-low trials were imposed. Among them, the low-to-high procedure did not yield exploitable results. Luckily, De Mooji's team exposed *Chlorella sorokiniana* to a low-to-high step. For the two successful tests, by fitting the experimental responses by a first-order model, one can obtain characteristic times of 8.06 ± 0.07 h for the high-to-low response and 9.85 ± 0.18 h for the low-to-high one. For the sake of simplicity, in this work, the average of the two timescales (τ_{Pig} = 8.96 h) will be considered as representing faithfully enough acclimation dynamic in both directions.

From this consideration, a differential equation governing the evolution of cell pigment concentration can be derived:

$$\frac{dY_{Pig}(t)}{dt} = \frac{1}{\tau_{Pig}}(Y_{Pig,Eq}(I_{Average}) - Y_{Pig}(t)) \tag{10}$$

where Y_{Pig} can be the cells chlorophyll a, b or lutein content and $Y_{Pig,Eq}(I_{Average})$ the associated equilibrium value obtained from experiments (Table 1), modeled as follows:

$$Y_{Pig,Eq}(I_{Average}) = A\ exp(-\frac{I_{Average}}{aI_{Average} + b}) \tag{11}$$

While purely empirical, this expression can adequately capture the sharp decrease of the cell pigment content between 25 and 100 μmolPhoton/m^2/s and the softer one exhibited afterward. Furthermore, it does not diverge when coming close to zero and does not tend towards zero when the illumination increases. All these traits allow it to mimic the experimental observations faithfully.

2.6.4. Temperature effect model

Microalgal growth, like microbial growth and most life-associated mechanisms, is temperature dependent [32]. Cold temperature tends to lower metabolic rate, too hot and freezing temperatures tend to harm the cells by irreversible denaturation of protein and DNA [8], and mechanical and/or osmotic stress [43], respectively. As a good rule of thumb, one could state that microalgae thrive between 15 and 35 °C. Still, precise studies covering a wide range of temperatures are lacking in the literature. Among the few, one can note the one from Sorokin, on *Chlorella sorokiniana* [44], and the one from Mayo, on *Chlorella vulgaris* [29]. Between the two, *Chlorella vulgaris* was preferred, as *Chlorella sorokiniana* was previously shown not to be the best-suited for biofaçade application in France [18]. Therefore, data from Mao et al. were fitted using the Cardinal Temperature Model with Inflection [45] (Eq. (12) and Fig. 3) to obtain the relative growth rate as a function of temperature.

$$\frac{\mu(T)}{\mu_{Max}} = \frac{(T - T_{Max})(T - T_{Min})^2}{(T_{Opt} - T_{Min})[(T_{Opt} - T_{Min})(T - T_{opt}) - (T_{Opt} - T_{Max})(T_{Opt} + T_{Min} - 2T)]} \tag{12}$$

2.7. Biological model augmentation

In addition to the basic formulation introduced above, several other aspects of microalgal phototropic growth were modeled to provide a more accurate description of the cells proliferation and assess the importance of such refinements.

2.7.1. Light vs. dark maintenance

Microalgal cell maintenance rate is known to vary with illumination. From a broad perspective, it can be categorized into two regimes:

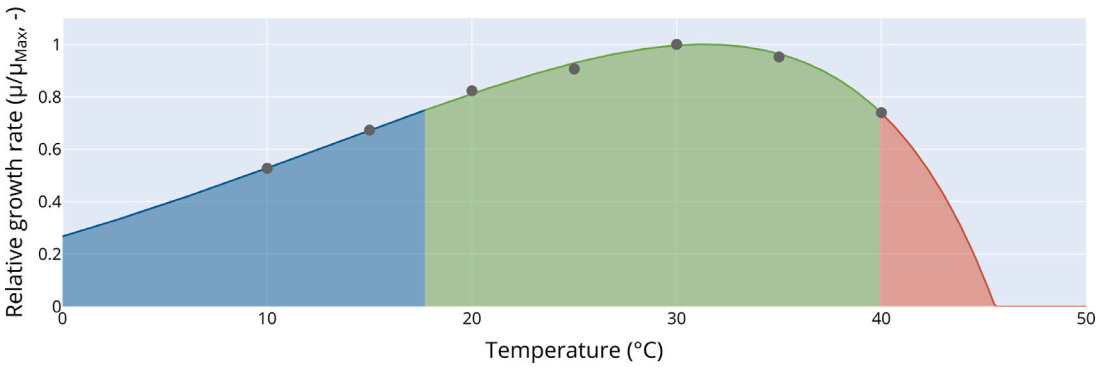

Fig. 3. Relative growth rate of *Chlorella vulgaris* as a function of temperature. Green area — relative growth rate between 75 and 100% of the maximal value. Blue area — relative growth rate below 75% on the cold side. Red area — relative growth rate below 75% on the hot side.
Source: Data extracted from [29].

light respiration and dark respiration [25,46]. The first one corresponds to high mitochondrial activity when the cells are exposed to light and proliferating. The second one is linked to resting metabolism. Of course, a transition between the two exists, and a dark period can be the place of intense metabolic activity, as in the case of synchronized cultures dividing during the dark part of the photoperiod [47]. Other refinements in the description of these modes can be noted. Among them, the dependence dark respiration rate upon cell light acclimation is of note [48]. Nevertheless, the modeling approach retained in this work acknowledged the complexity of the phenomena at stake and decided to adopt a humble position with respect to the extent of the unknown surrounding them. Two hypotheses were tested:

- a constant maintenance rate taken as the light respiration, as the night may be the place for metabolic processes (like in the case of synchronized cultures),
- a variable maintenance rate switching between light respiration during daytime and dark respiration during nighttime, describing the night period as a resting time.

Finally, values for the submodels implementation were drawn from experiments where the authors measured light respiration over 22 days ($3.88\ 10^{-2} \pm 1.79\ 10^{-3}$ 1/day) and dark respiration over 73 days ($7.42\ 10^{-3} \pm 3.33\ 10^{-3}$ 1/day) for *Chlorella vulgaris* [25].

2.7.2. Absorption cross section & cell pigment content

After determining the importance of how maintenance is accounted for, the next refinement is to link to cell pigment contents to their absorption cross section. This can easily be done by assuming an intrinsic cross section of chlorophyll and multiplying by the total amount of chlorophyll hosted by a cell (Eq. (13), with $\sigma_{Abs,Chl} = 20.3\ 10^3$ $m^2/kg_{Chl\ Total}$ as an average value over the visible spectrum, based on Baránková et al.'s observations). While this method does not take into account cell illumination history, it can be deemed precise enough for the intended use [39].

$$\sigma_{Abs} = \sigma_{Abs,Chl} Y_{Chl\ Total} \tag{13}$$

2.7.3. Light spectral distribution

The last refinement introduced in the model takes into consideration the fact that cell light absorption varies across the visible spectrum. It is comparatively more important in the blue (400 to 500 nm) and red (600 to 750 nm) regions than in the green one (500 to 600 nm). Therefore, it is possible to subdivide the visible light into these three bands. This will notably affect Eq. (1), (2), and (13), which will have to evolve to take into account the spectral distribution. For example, the equation governing the absorbed power is altered in the following way:

Table 2
Absorption cross section value for the whole visible spectrum and the blue (400 to 500 nm), green (500 to 600 nm), and red (600 to 750 nm) bands. Data extracted from [39] and [40] for the values specific to the dry weight (presented as average ± half span). Data extracted from [39] for the values specific to the chlorophyll content.

	Whole spectrum	Blue	Green	Red
$\sigma_{Abs,\lambda}$ (m^2/kg_{DW})	253 ± 2	480 ± 4	110 ± 2	185 ± 2
$\sigma_{Abs,Chl,\lambda}$ (m^2/kg_{Chl})	16.5 10^3	31.5 10^3	7.31 10^3	12.0 10^3

$$Phi_{Abs} = \frac{SPhi_{Inc,Vis}}{3} \sum_{\lambda=R,G,B} (1 - exp(-\sigma_{Abs,\lambda} X L)) = \frac{SI_0 k}{3} \sum_{\lambda=R,G,B} (1 - exp(-\sigma_{Abs,\lambda} X L)) \tag{14}$$

where $\sigma_{Abs,\lambda}$ is the light absorption cross of the cells within blue, green, and red ranges of the visible spectrum (power assumed distributed equally between these bands). In the same manner, the cross section specific to the cell chlorophyll concentration can also be divided according to the visible spectrum components. The different values are summarized in Table 2.

2.8. Illustration case — description

Once the model is introduced and implemented (Python 3.10), a test case is to be chosen to explore its behavior and the importance of its potential refinements. In this case, the best performing configuration identified in previous work, focusing on the thermal aspects only, will be used as the reference (summarized in Table 3). Regarding time span and location, the biofaçade will be assumed to be located in Marseille city (South of France), and the analysis will cover the whole year 2023. In addition, an element characterizing the bioprocess operation has to be added: the dilution applied when the transmitted light falls below the prescribed value (75%). For the purpose of this illustration, it will be considered that 20% of the culture will be replaced by fresh medium. While this operation mode can be guessed suboptimal beforehand, it was chosen as it is the most challenging to model and creates the most contract between the model augmentations. Of course, the present model opens the way to determining more relevant design and operation procedures supported by actual biotechnological performance. However, this endeavor is a sizable amount of work. Hence, it is the topic of the companion article. Moreover, it is also important to acknowledge some limitations of the model. By its nature, *i.e.*, assuming that pH is always maintained in a range adequate for *Chlorella vulgaris* growth (*i.e.*, 5 to 8.5 [29]), proper supply of nutrients, and absence of aggressive bacterial contamination, the model can be used for design purposes or techno-economical analysis. On the contrary, actual system supervision lies outside the scope in its current form and would require extensive validation against experimental work on dedicated facilities.

Table 3
Key geometrical, physical and bioprocess parameters describing the reference case.

Design parameters and operating procedures	Reference value	Unit
Elevation of the biofaçade above the ground	20	m
Width of the biofaçade	1	m
Height of the biofaçade	4	m
Thickness of the biofaçade reservoir (L)	0.08	m
Number of outdoor glazing	2	–
Green light transmitted fraction	75	% of incident light
Sparged gas origin	Building	–
Use of boiler fume	Yes	–
Orientation	South	–
Strain type	*Chlorella vulgaris*	–
Radiative film type	Greenhouse	–
Volume replacement	20	% of total volume

3. Numerical methods

3.1. Initial conditions & numerical transient duration

Initial conditions for variables governed by differential equations (temperature, biomass concentration, ...) were obtained by running the model over the whole year 2022. After checking that the system has had the expected behavior, the values were selected among the ones encountered at the end of the year. This procedure ensures that the values are within the system's normal operating range and prevents the occurrence of an artificially long ramping-up.

As a biofaçade is envisioned as a system running continuously of the year, it is mandatory to question the duration of the transient period to be discarded at the beginning of the simulation to ensure no effect from the initial condition [49]. Thus, transient periods up to 10 weeks were tested. The tests revealed that the duration influenced by the initial condition was below one week. Indeed, for all the tested duration, outputs (biomass and pigment productions) fluctuate below 0.5% of their mean value. The explanation is relatively straightforward: the system requires less than one week to reach the cell concentration to trigger a dilution. Consequently, a transient period of at least three weeks was selected, as exploring possible configurations could slightly modulate this conclusion, and the extra computational cost is marginal.

3.2. Uncertainty management

Previous investigations have showed that uncertainty surrounding the value of some physical parameters could have a non negligible impact on the thermal behavior of the system [18,19]. Notably, a global sensitivity analysis identified microalgae culture emissivity and indoor building emissivity as the primary drivers of variability. Additionally, surrounding emissivity was found to act as a potential modulator. Consequently, a Monte Carlo approach was deployed to address this uncertainty. In this approach, the model was executed multiple times for a given configuration, with microalgae culture emissivity (ϵ_{mc}), building indoor emissivity (ϵ_{In}), and surrounding emissivity (ϵ_{Sur}) sampled from uniform distributions (ranging between 0.8 and 1.0, 0.5 and 0.7, and 0.8 and 1.0, respectively). This process generated a distribution of performance metrics, from which average performances and associated standard deviations were derived. To ensure effective convergence, values were sampled using a Sobol's sequence, known for its ability to explore hypercubes uniformly and facilitate rapid and accurate convergence while minimizing computational load [50]. One could argue that such sequences tend to be conservative, treating extreme configurations as equally likely as central ones, thus reinforcing the robustness of the conclusions. A convergence analysis (detailed in the Supplementary Materials) concluded that 256 iterations were sufficient to produce stable estimates of averages and standard deviations for all indicators detailed in the next Section.

3.3. Outputs & analysis

In the context of the present work, a microalgae biofaçade system can be deemed to have four main outputs: the produced biomass and the three pigments describing cells composition. Among the four, two will be highlighted: biomass, as it is the primary production and can relate to financial and environmental assessment, and cell lutein content. Indeed, in general, biomass quality can be assessed using cell pigment or lipid contents [51]. Lutein was chosen as it is a high-value molecule of primary interest for human health lacking in western diet [52]. In terms of the methodology for analysis of the system performances, the ANOVA framework could be resorted to. Yet, the high number of runs makes this approach irrelevant [53] as all differences appear statistically significant. Therefore, effect size and effect size indices (such as Cohen's d [53,54]) will be used to drive the analysis. Cohen's d provides a comparison of two populations' means, taking into account their standard deviations (Eq. (15)). In terms of interpretation, an absolute Cohen's d value below 1 suggests that the two population are distant by less than one standard deviation (hence quite close), a value above 4 suggests clearly segregated populations.

$$d = \frac{\bar{X_1} - \bar{X_2}}{\sqrt{\frac{s_1^2 + s_2^2}{2}}} \tag{15}$$

4. Results and discussion

4.1. Illustration case — analysis

The operation of a microalgae biofaçade located in Marseille over 2023 was chosen as an illustration case for this model. The operational procedure was to trigger a dilution by 20% when the transmitted fraction of the green part of the visible spectrum fell below 75%. This procedure ensures that the building workers benefit from adequate lighting at the detriment of the culture, which is far from harnessing all the light it could. Nevertheless, may the kind reader keep in mind that the purpose of this scenario is to showcase the model capabilities, not to optimize the system. For this very reason, all the augmentations were enabled during the computation of this test case.

Fig. 4 presents the culture density and microalgae lutein content over 2023. As one can see, the culture was subjected to numerous dilutions, and biomass concentration and lutein content evolved accordingly. The lutein content falls to a minimum of 2 mg/g after a dilution as the low biomass concentration and the high resulting illumination drew biomass to reduce its pigment content. Subsequently, it reaches about 6 mg/g when the culture grows dark again.

In addition to the observed short-term pattern (over a few days), a longer one is also noticeable (year-round). During summertime, the biomass concentration is higher, and its pigment content is lower. However, before dissecting the mechanisms, it is important to recall that incident illumination on a vertical surface is lower in summer than in winter [19]. In addition, the daytime duration is longer in summer than in winter. These two phenomena have adverse effects. on the one hand, a lower illumination drives the cells towards a higher equilibrium pigment content during daytime. Even though this value remains far below the one during nighttime, this observation advocates for an increase in cell pigment content over the summertime. On the other hand, the fact that the days are longer during this period of the year leaves more time for the cell to downregulate their pigment content during daytime. From the model predictions, it is this last phenomenon that drives the pigment profile dynamic. Consequently, during summertime, biomass pigment content is lower and a higher biomass concentration can attenuating incident light enough to trigger a dilution. During winter, it is the opposite. Hence, the biomass has a higher pigment content. Thus, a lower concentration is required to trigger a dilution.

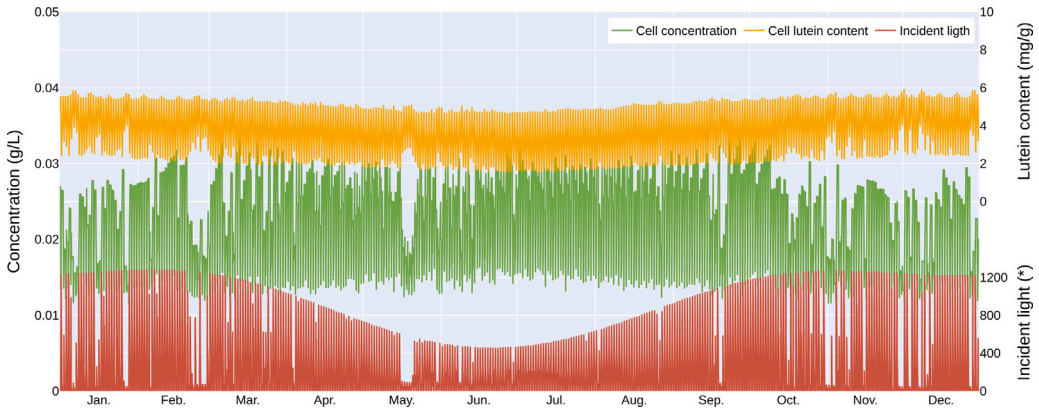

Fig. 4. Culture density, microalgae lutein content, and incident illumination over the year 2023. * μmolPhoton/m^2/s.

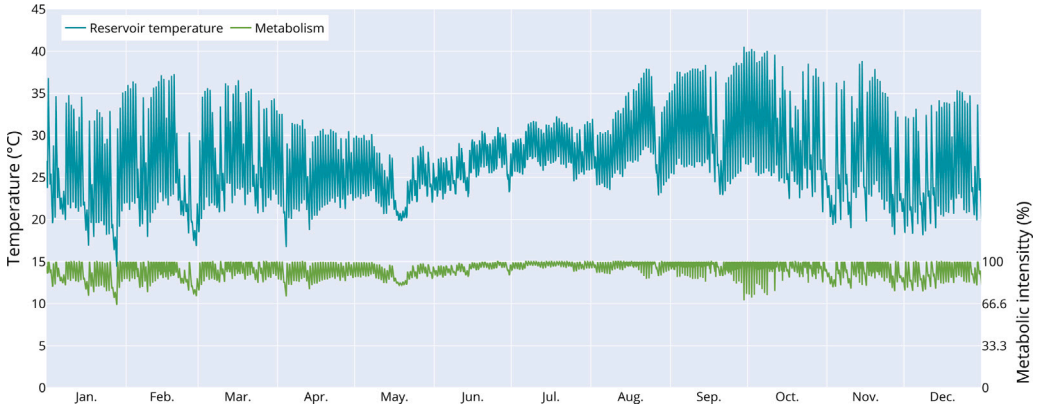

Fig. 5. Culture temperature and metabolic rate (relative to the maximum) over the year 2023.

Another aspect of the model is the interplay between culture temperature and metabolic rate. Both are graphed in Fig. 5. As one can see, the culture temperature fluctuates widely, between 11 °C (on a very time-limited episode at the end of January) and (38 °C at the end of September 2023). While the amplitude of the variation is considerable (27 °C), the resulting metabolic rate is relatively stable and high. Indeed, the minimum value lies at 66% of the maximal rate, with a first decile at 85% and a median as high as 95%. Nevertheless, like biomass production and cell lutein content, a pattern exists between the hot and the cold season.

To investigate it further, Fig. 6 focuses on two weeks, one in January (cold season) and one in July (hot season). Two sets of values are displayed; one is extracted from the simulation representing the culture condition, and the other is a hypothetical setting assuming that the culture has the same temperature as the outdoor air. The objective is to assess the magnitude of the synergy between the building and the biofaçade. The hot season configuration is straightforward to analyze. The biofaçade offers a temperature similar to that of the outdoor air, which is well-suited for microalgae cultivation. Hence, metabolic rates are similar and relatively high. These observations substantiate the gain offered by integrating photobioreactors into a building façade.

Still, significant differences emerge during the cold season. First, the magnitude of the temperature fluctuations is wider. Second, the biofaçade allows the culture temperature to increase by 15 °C on sunny days (first part of the portrayed week) and by 5 °C on cloudy days (second part of the week). These temperature increases are all the more welcome as the outdoor temperature falls below 15 °C, a temperature below which *Chlorella vulgaris* metabolic rate drops rapidly (Fig. 3). Consequently, when placed within a biofaçade, the culture metabolic rate oscillates around 91 ± 5% (average value ± standard deviation), while it would fluctuate around 58 ± 9% if left outdoors.

Finally, year-round consolidated indicators are also of interest. The overall biomass production stands at 2.05 kg and the lutein production at 9.43 g. This modest performance can be explained by the low absorption of impinging light (25%) and the relatively high illumination within the culture (305 μmolPhoton/m^2/s, on average during daytime), which lowers the photoconversion efficiency. Optimizing the system, as explored in the companion article, allows easily the achievement of biomass and lutein productions higher than 18 kg and 110 g, respectively, but this lies outside the scope of the present article.

4.2. Sub-model influence

As the proposed model features several refinements, their relative contributions to the overall prediction are to be investigated. To do so, all the augmentations were systematically turned on and off to discriminate their importance. Overall, eight combinations were evaluated, as three augmentations with two levels each have been introduced (variable maintenance rate as a function of day and night, absorption cross section as a function of cell pigment content, and absorption cross section as a function of the wavelength). Fig. 7 proposes a violin plot of the system outputs for every possible combination. The results focus on biomass and lutein production. Furthermore, they are graphed as distribution because uncertain parameters (*e.g.*, culture emissivity) were distributed following a Sobol sequence to account for the unknown tied to their values.

Focusing on biomass production, variable maintenance rate and light absorption cross section depending on cell pigment content do

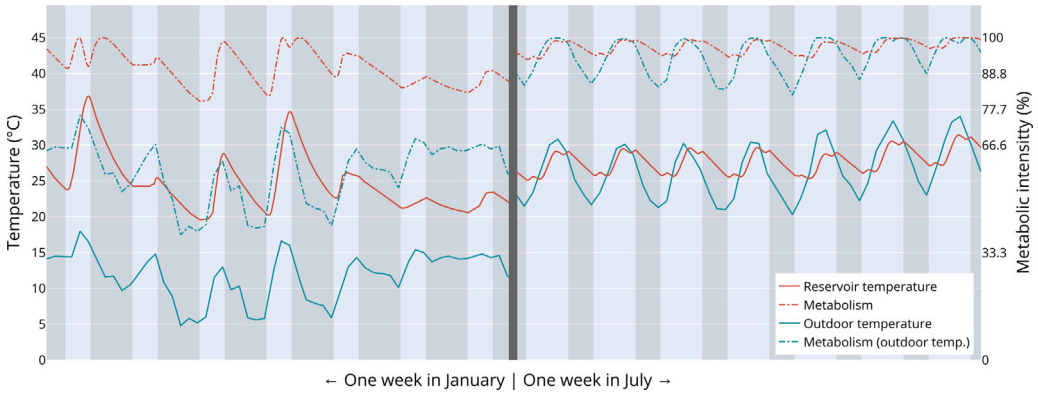

Fig. 6. Culture temperature and metabolic rate (relative to the maximum) for a culture hosted by a biofaçade (red) or placed outside (blue, assumed to be at the same temperature as the outdoor air). On the left, a week during the cold season, on the right, a week during the hot season.

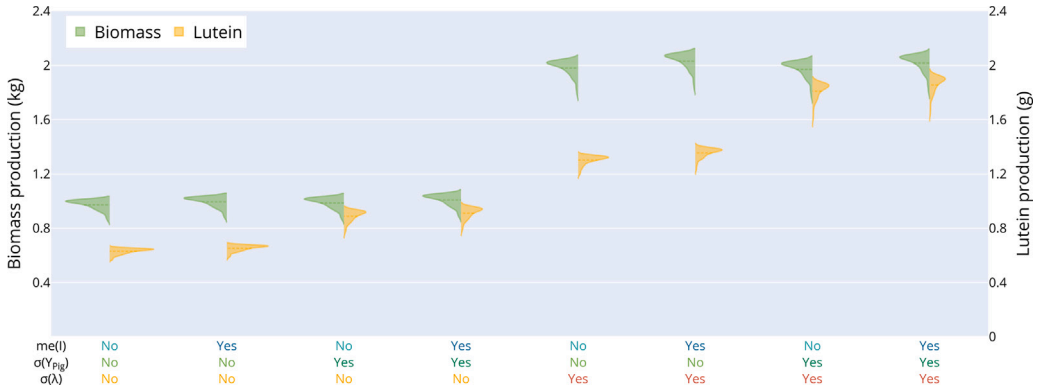

Fig. 7. Biomass and lutein production for the different combinations of the model augmentations.

not impact significantly the outcome (group-wise, Cohen's d below 1 for the four firsts and four last combinations). This can be explained by the fact that the maintenance rate, either taken as light or dark respiration, is much lower than cell production. Hence, its modulation does not influence much the outcome. Regarding absorption cross section dependency on cell pigment content, overall, it does not modulate significantly the absorbed energy (2.37 GJ vs. 2.43 GJ, with or without, over 2023). Hence, biomass production is not altered. In an opposite manner, accounting for the absorption cross section's spectral properties substantially modulates the system biomass production (Cohen's d above 4). Indeed, improving the description of light absorption in the green region (which is lower than the average absorption over the visible spectrum) allows the culture to harness more light energy (4.47 GJ vs. 2.43 GJ, with or without, over 2023) and produce more biomass. Still, while impressive, one should keep in mind that this effect is a direct consequence of the bioprocess control procedure: triggering a dilution when green light transmittance falls below a threshold (75% in the present case). Another procedure, such as the dilution triggered as fixed intervals, as explored in the companion article, would yield less contrasting results (8.1% difference). However, it would not underline the implication of this model refinement to its fullest.

Focusing on lutein production, the variable maintenance rate is the only refinement which influence is negligible (Cohen's d below 1). Indeed, it does not interplay with cell pigment content and only marginally affects cell production. Hence, lutein production is relatively unaffected by this augmentation. In a parallel manner, describing absorption cross section as a function of the wavelength increases biomass production while not modulating the cell pigment content. However, the sole increase in biomass production drives lutein production. Finally, the case of the indexation of the absorption cross section of the pigment content is more subtle to decipher. To trigger a dilution, the system requires two things: a culture dense enough (either by a large amount of biomass, a large cell pigment content, or both) and light (to determine the transmitted fraction). Hence, nighttime plays a peculiar role. It drives cells to increase their pigment content while preventing a culture dilution (no light to measure the transmitted fraction). The resulting behavior is that flushes are more frequent in the early morning when cells exhibit a high pigment content. Indexing of the absorption cross section of the pigment content amplifies this behavior, hence the pigment production. Leaving the technical analysis aside for a second, one could note that this procedure increases the production of quality microalgal biomass, *i.e.*, with a higher pigment content.

The above analyses have focused on explaining each model augmentation contribution to the overall outcome. Yet, while informative, Fig. 7 is not the best-suited tool for a thorough analysis. Indeed, in addition to the effect of each refinement, the question of their potential couplings also needs to be addressed. An effect analysis was carried out to investigate them based on the systematic activation/deactivation of the model augmentations. The results are summarized in Table 4. Effects values confirm that biomass production is only affected by the absorption cross section wavelength dependency. Pigment productions are confirmed to be influenced by the cross section description refinements but also by their interaction in an additive manner. Finally, improving maintenance description does not influence any of the outcomes, neither as a main factor nor through interactions.

Overall, it can be concluded from this analysis of the model refinements that account for absorption cross section dependencies on pigment content and wavelength are important. Regarding maintenance rate, while it is of theoretical and biological interest, its improved description does not appear key from a practical perspective.

Table 4
Effect of refinement (and combinations) of the model of the four outputs. In bold, the one above 5% of the intercept, to ease reading.

	Production over 2023			
	Biomass (kg)	Chlorophyll a (g)	Chlorophyll b (g)	Lutein (g)
Intercept	1.49	25.69	12.3	5.87
me(I)	0.03	0.74	0.35	0.18
$\sigma(Y_{Pig})$	0.00	**6.49**	**3.07**	**1.91**
$\sigma(\lambda)$	**1.01**	**17.76**	**8.50**	**4.05**
me(I) × $\sigma(Y_{Pig})$	0.00	−0.04	−0.02	−0.01
me(I) × $\sigma(\lambda)$	0.01	0.28	0.14	0.07
$\sigma(Y_{Pig})$ × $\sigma(\lambda)$	−0.01	**2.01**	**0.95**	**0.62**
me(I) × $\sigma(Y_{Pig})$ × $\sigma(\lambda)$	0 .00	−0.03	−0.01	−0.01

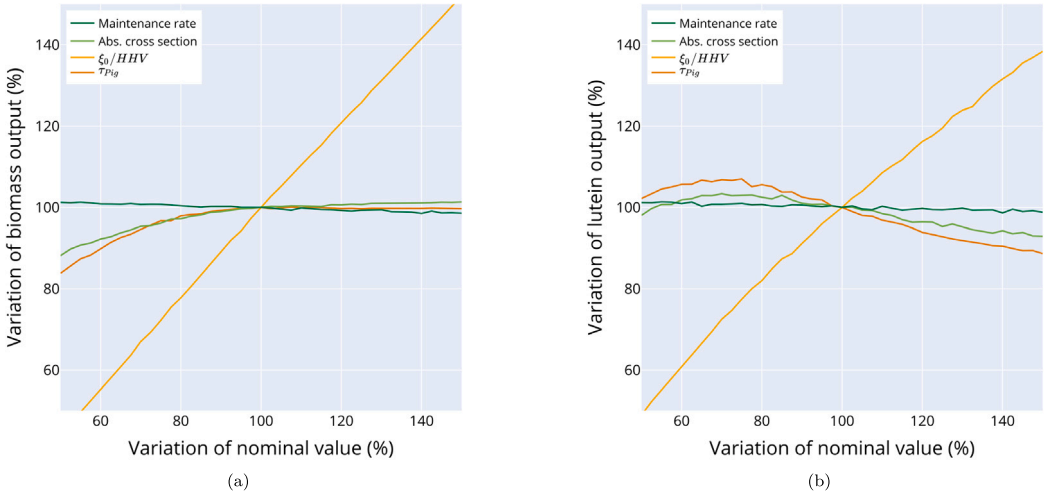

Fig. 8. Local sensitivity analysis. Left — gross growth rate. Right — cell lutein content.

4.3. Biological parameter local sensitivity analysis

Once the importance of the different model variations has been weighted, the influence of the parameters driving the model is to be analyzed. To do so a local sensitivity analysis was carried out. Four parameters were screened independently: the maintenance rate, the absorption cross section value, the ξ_0/HHV ratio, and the pigment expression characteristic time. All parameters were varied within ± 50% of their nominal values, with a 2.5% step. The resulting variations in the biomass and lutein productions are graphed in Fig. 8. Unsurprisingly, given the above considerations, varying maintenance rate has almost no perceivable effect. The two pigment-related parameters induce a similar response. They lightly modulate biomass production when selected below 80% of their nominal values. Their increase lowers lutein production by lowering the overall cell pigment content required to trigger a dilution (which happen at the same frequency). The opposite is observed when decreasing their values. However, below 70% of their nominal values, the decrease in biomass production counters the increasing trends and drives lutein production downward. Finally, the ξ_0/HHV ratio, which lies at the heart of biomass production, affects almost linearly the system outcomes.

4.4. Key parameters global sensitivity analysis

Once modeling choices have been evaluated and local sensitivity analysis performed on biological parameters, it is time to take a step back and evaluate the system's robustness as a whole. To do so, global sensitivity analyses may be the best-suited tool. Indeed, they examine the influence of selected parameters over a wide range of configurations (by combining the uncertainty of all the selected parameters). Among these methods, Sobol's indices method stands out for its ease of deployment and interpretation [55]. In a nutshell, numerous combinations of parameter values are generated (about 60 thousand here), and an ANOVA regression is conducted to determine the amount of variance associated with each of the parameters and their interactions. In our case, the selected parameters, based on the previous analyses, and their ranges are presented in Table 5. Among them, photoconversion efficiency is of particular interest, as the local sensitivity analysis showed its importance. Its range of variation was determined based on the uncertainty tied to ξ_0 (0.61 %, based on the reported values [22–25], for a reference value of 4.34%) and HHV (0.30 MJ/kg for a reference value of 20.51 MJ/kg). Combined together, under the random error assumption, they suggest that the ξ_0/HHV ratio could vary between ±12.7% of its nominal value. Hence, a ±15% variation range was chosen. Finally, a uniform sampling approach was used to draw parameter values from the presented intervals before running the model.

Table 5
Parameters selected for the Sobol's indices analysis and their explored range of variation. Samples drawn following a Sobol sequence.

Description & Symbol	Nominal value & Unit	Range
Photoconversion (ξ_0/HHV)	2.12 10^{-9} kg/J	±15%
Pigment expression characteristic time (τ_{Pig})	8.96 - h	±20%
Absorption cross section (σ)	Varying	±20%
Indoor emissivity (ϵ_{In})	0.7	[0.6–0.8]
Microalgae culture emissivity (ϵ_{mc})	0.9	[0.8–1.0]
Surrounding emissivity (ϵ_{Sur})	0.9	[0.8–1.0]

Fig. 9 - top - presents the results from the global sensitivity analysis. The first comment is that for both biomass and pigment productions, the standard deviation of the predictions lies within 10% of the average of the distribution. The model prediction can, therefore, be deemed quite robust. Then, focusing on the uncertainty origin, one can see that the ξ_0/HHV ratio is the dominant source. This observation is in good

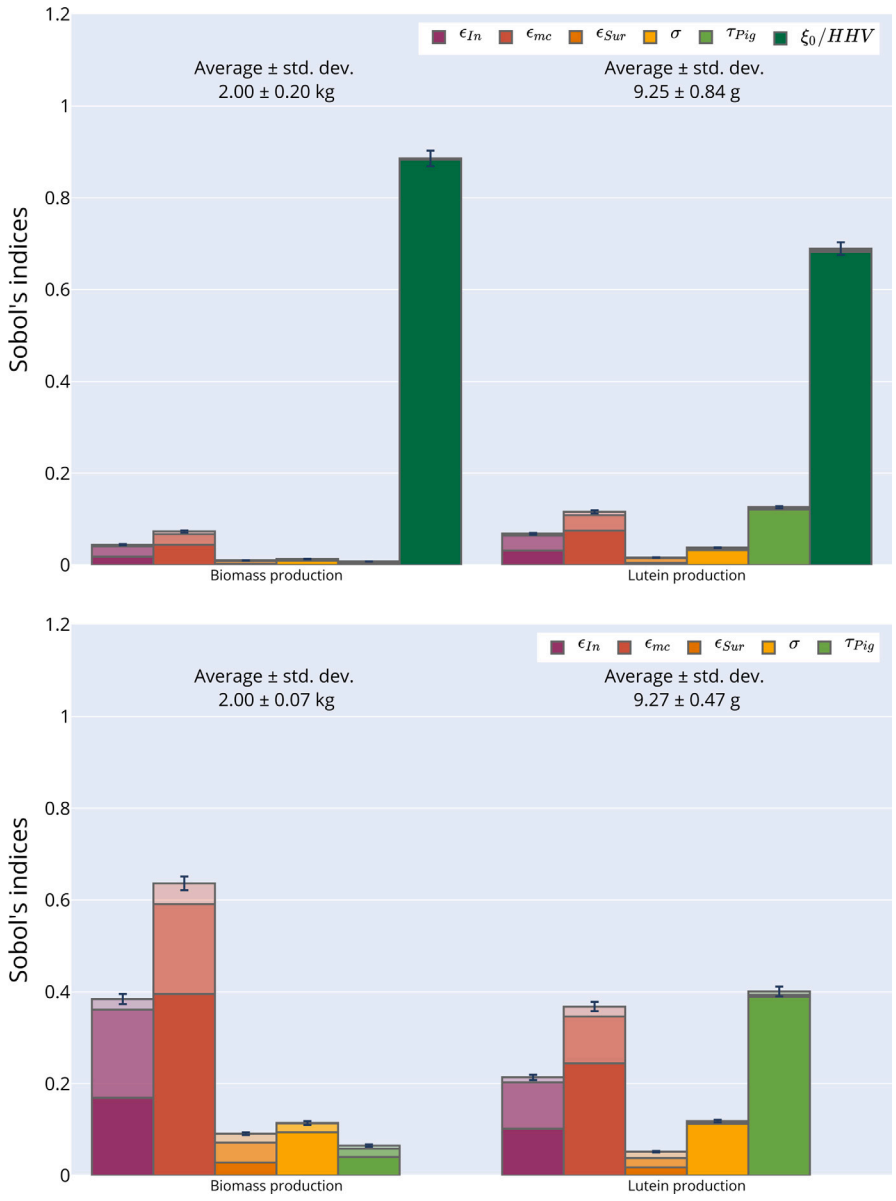

Fig. 9. Sobol's indices in the illustration case configuration. Top — considering all the variables. Bottom — removing ξ_0/HHV from the selection. Solid bars — first order indices. Shaded bars — second order indices. Almost empty bars — total order with confidence interval.

agreement with the local sensitivity analysis. This parameter should, therefore, be finely evaluated before designing a microalgae biofaçade system. Nevertheless, the other parameters also act as modulators. For example, the building indoor emissivity and the culture emissivity influence biomass production. Furthermore, biomass production and pigment production sensitivities feature resembling, yet different, profiles. For example, pigment expression characteristic time modulates pigment production contrary to biomass production.

Finally, it is also interesting to analyze the system sensitivity under the assumption that one has ascertained the value of the ξ_0/HHV ratio. Fig. 9 - bottom — illustrates the Sobol's indices in this configuration. First, one can note that the overall variability is about halved (down to 3.5% for biomass production and 5% for lutein production). Second, all the parameters come into play to build the variability in the system outcomes. They also feature a high level of interaction (second-order indices and above). Biomass production is mostly impacted by thermal properties, while lutein production is vastly influenced by the pigment expression dynamic. This last analysis underlines the very high level of intrication between the thermal and biological aspects of a microalgae biofaçade. This ultimately underlines the relevance of modeling as a tool to decipher and optimize such a complex system.

5. Conclusion

This article presented the development of a model coupling the thermal and biological behaviors of a microalgae biofaçade. Heat fluxes and illumination were modulated by actual weather data, and the system response was addressed in terms of biomass and pigment production. First, the effect of the different model refinements were screened. Then, the model was applied to an illustrative case: the city of Marseille over the year 2023. Analyzing the results illustrated the model's capabilities: assessing the building/biofaçade thermal synergy or the summer/winter operational differences. The numerical behavior of the model was also analyzed: local and global sensitivity analyses assessed the impact of uncertain parameters. The parameter inducing the highest amount of uncertainty is the microalgae photoconversion efficiency, highlighting the need to ascertain its value before designing a system. Nevertheless, even under conservative assumptions, the predictions of

the model are 10% accurate. Consequently, it is with high confidence that this model can be used in a companion paper to design a biofaçade numerically.

Nomenclature

Latin symbols	Property	Unit
a	Shape factor	–
b	Shape factor	μmolPhotonPAR/m^2/s
d	Cohen'd	–
HHV	Higher Heating Value	MJ/kg
I_0	Incident photosynthetically active light intensity	μmolPhotonPAR/m^2/s
k	Conversion factor	μmolPhotonPAR/J
L	Characteristic length	m
me	Maintenance rate	1/day
S	Surface	m^2
s	Standard deviation	Varying
T	Temperature	°C in the text/K in formulas
V	Volume	m^3
X	Cell concentration	kg/m^3
Y	Pigment content	mg/g

Greek symbols	Property	Unit
ϵ	Emissivity	–
μ	Microalgae growth rate	1/day
σ	Cross section	m^2/kg
τ	Characteristic time	s
Φ	Heat flux	W/m^2
ξ	Photosynthetic efficiency	–

Subscript	Description
Abs	Absorbed by the culture
Average	Average over the volume
Chl	Chlorophyll
Conv	Convective-conductive
Eq	Equilibrium
Gas	Sparged gas
Gross	Gross
In	Indoor
Inc	Incident
Inlet	Gas injection
Max	Maximum
mc	Microalgae culture
Min	Minimum
Net	Net
Opt	Optimal
Out	Outdoor
Outlet	Gas vent
Pig	Pigment
Rad	Radiative
Ref	Reference
Sky	Sky
Sun	Sun
Sur	Surrounding
Total	Total
Vis	Visible
λ	Wavelength band
0	At I = 0 μmolPhotonPAR/m^2/s

CRediT authorship contribution statement

Victor Pozzobon: Writing – review & editing, Writing – original draft, Visualization, Validation, Supervision, Software, Resources, Project administration, Methodology, Investigation, Formal analysis, Data curation, Conceptualization.

Declaration of competing interest

The authors declare that they have no known competing financial interests or personal relationships that could have appeared to influence the work reported in this paper.

Acknowledgments

Communauté urbaine du Grand Reims, Département de la Marne, Région Grand Est and European Union (FEDER Grand Est 2021–2027) are acknowledged for their financial support to the Chair of Biotechnology of CentraleSupélec and the Centre Européen de Biotechnologie et de Bioéconomie (CEBB).

Appendix A. Supplementary data

Supplementary material related to this article can be found online at https://doi.org/10.1016/j.renene.2024.121545.

Data availability

A Python implementation of the proposed model is freely available at https://github.com/victorpozzobon/biofacade.

References

[1] S. Díaz, J. Settele, E. Brondizio, H.T. Ngo, M. Guèze, J. Agard, C. Zayas, IPBES global assessment: summary for policymakers, 2019, Retrieved from IPBES website: https://www.ipbes.net/news/ipbes-global.
[2] M. Rizwan, G. Mujtaba, S.A. Memon, K. Lee, N. Rashid, Exploring the potential of microalgae for new biotechnology applications and beyond: A review, Renew. Sustain. Energy Rev. 92 (2018) 394–404.
[3] W. Levasseur, P. Perré, V. Pozzobon, A review of high value-added molecules production by microalgae in light of the classification, Biotech. Adv. 41 (2020) 107545.
[4] H.R. Molitor, E.J. Moore, J.L. Schnoor, Maximum CO2 utilization by nutritious microalgae, ACS Sustain. Chem. Eng. 7 (10) (2019) 9474–9479, Publisher: American Chemical Society.
[5] N. Brown, A. Shilton, Luxury uptake of phosphorus by microalgae in waste stabilisation ponds: current understanding and future direction, Rev. Environ. Sci. Bio/Technol. 13 (3) (2014) 321–328.
[6] J.A. Hellebust, I. Ahmad, Regulation of nitrogen assimilation in green microalgae, Biol. Oceanogr. 6 (3–4) (1989) 241–255, Publisher: Taylor & Francis _eprint: https://www.tandfonline.com/doi/pdf/10.1080/01965581.1988.10749529.
[7] P.K.C. Sasi, J.M. AmbilyViswanathan, D.M. Thomas, J.P. Jacob, S.V. Paulose, Phycoremediation of paper and pulp mill effluent using planktochlorella nurekis and chlamydomonas reinhardtii–A comparative study, J. Environ. Treat. Tech. 8 (2) (2020) 809–817.
[8] T.D. Brock, Life at high temperatures, Science 230 (4722) (1985) 132–138.
[9] M. Talaei, M. Mahdavinejad, R. Azari, Thermal and energy performance of algae bioreactive façades: A review, J. Build. Eng. 28 (2020) 101011.
[10] R. Mahrous, E. Giancola, A. Osman, T. Asawa, H. Mahmoud, Review of key factors that affect the implementation of bio-receptive façades in a hot arid climate: Case study north Egypt, Build. Environ. 214 (2022) 108920.
[11] J. Pruvost, B. Le Gouic, O. Lepine, J. Legrand, F. Le Borgne, Microalgae culture in building-integrated photobioreactors: Biomass production modelling and energetic analysis, Chem. Eng. J. 284 (2016) 850–861.
[12] E.S. Umdu, I. Kahraman, N. Yildirim, L. Bilir, Optimization of microalgae panel bioreactor thermal transmission property for building façade applications, Energy Build. 175 (2018) 113–120.
[13] C. Barajas Ferreira, L. Castro Padilla, G.V. Sánchez, A.D. González-Delgado, a.F. Barajas Solano, Design of a microalgae bio-reactive facade reactor for cultivation of Chlorella vulgaris, Contemp. Eng. Sci. 10 (2017) 1067–1074, Accepted: 2021-12-01T16:34:12Z Publisher: Contemporary Engineering Sciences.

[14] A.M. Elmalky, M.T. Araji, Computational fluid dynamics using finite volume method: A numerical model for double skin façades with renewable energy source in cold climates, J. Build. Eng. 60 (2022) 105231.
[15] A.M. Elmalky, M.T. Araji, Multi-objective problem of optimizing heat transfer and energy production in algal bioreactive façades, Energy 268 (2023) 126650.
[16] E. Todisco, J. Louveau, C. Thobie, E. Dechandol, L. Hervé, S. Durécu, M. Titica, J. Pruvost, A dynamic model for temperature prediction in a façade-integrated photobioreactor, Chem. Eng. Res. Des. 181 (2022) 371–383.
[17] F. Girard, C. Toublanc, Y. Andres, E. Dechandol, J. Pruvost, System modeling of the thermal behavior of a building equipped with facade-integrated photobioreactors: Validation and comparative analysis, Energy Build. 292 (2023) 113147.
[18] V. Pozzobon, Microalgae bio-reactive façade: A radiative-convective model powered by hourly illumination computation and historical weather data, J. Build. Eng. 90 (2024) 109407.
[19] V. Pozzobon, Microalgae bio-reactive façade: Location and weather-based systematic optimization, Build. Environ. 253 (2024) 111352.
[20] H. Sarmadi, M. Mahdavinejad, A designerly approach to Algae-based large open office curtain wall Façades to integrated visual comfort and daylight efficiency, Sol. Energy 251 (2023) 350–365.
[21] F. Ahmadi, S. Wilkinson, H. Rezazadeh, S. Keawsawasvong, Q. Najafi, A. Masoumi, Energy efficient glazing: A comparison of microalgae photobioreactor and Iranian Orosi window designs, Build. Environ. 233 (2023) 109942.
[22] J. Wurm, M. Pauli, SolarLeaf: The world's first bioreactive façade, arq: Archit. Res. Q. 20 (1) (2016) 73–79, Publisher: Cambridge University Press.
[23] I. Wagner, C. Steinweg, C. Posten, Mono- and dichromatic LED illumination leads to enhanced growth and energy conversion for high-efficiency cultivation of microalgae for application in space, Biotechnol. J. 11 (8) (2016) 1060–1071, _eprint: https://onlinelibrary.wiley.com/doi/pdf/10.1002/biot.201500357.
[24] R. Dillschneider, C. Steinweg, R. Rosello-Sastre, C. Posten, Biofuels from microalgae: Photoconversion efficiency during lipid accumulation, Bioresour. Technol. 142 (2013) 647–654.
[25] A. Oliver, C. Camarena-Bernard, J. Lagirarde, V. Pozzobon, Assessment of photosynthetic carbon capture versus carbon footprint of an industrial microalgal process, Appl. Sci. 13 (8) (2023) 5193, Number: 8 Publisher: Multidisciplinary Digital Publishing Institute.
[26] C. Safi, B. Zebib, O. Merah, P.-Y. Pontalier, C. Vaca-Garcia, Morphology, composition, production, processing and applications of Chlorella vulgaris: A review, Renew. Sustain. Energy Rev. 35 (2014) 265–278.
[27] V. Pozzobon, Chlorella vulgaris cultivation under super high light intensity: An application of the flashing light effect, Algal Res. 68 (2022) 102874.
[28] W. Levasseur, P. Perré, V. Pozzobon, Chlorella vulgaris acclimated cultivation under flashing light: An in-depth investigation under iso-actinic conditions, Algal Res. 70 (2023) 102976.
[29] A.W. Mayo, Effects of temperature and pH on the kinetic growth of unialga chlorella vulgaris cultures containing bacteria, Water Environ. Res. 69 (1) (1997) 64–72, _eprint: https://onlinelibrary.wiley.com/doi/pdf/10.2175/106143097X125191.
[30] A.M. Elmalky, M.T. Araji, Optimization models for photosynthetic bioenergy generation in building façades, Renew. Energy 228 (2024) 120607.
[31] T. Defraeye, J. Carmeliet, A methodology to assess the influence of local wind conditions and building orientation on the convective heat transfer at building surfaces, Environ. Model. Softw. 25 (12) (2010) 1813–1824.
[32] Q. Béchet, A. Shilton, B. Guieysse, Modeling the effects of light and temperature on algae growth: State of the art and critical assessment for productivity prediction during outdoor cultivation, Biotech. Adv. 31 (8) (2013) 1648–1663.
[33] S. Esposito, V. Botte, D. Iudicone, M. Ribera d'Alcala', Numerical analysis of cumulative impact of phytoplankton photoresponses to light variation on carbon assimilation, J. Theoret. Biol. 261 (3) (2009) 361–371.
[34] J. Hoeniges, W. Welch, J. Pruvost, L. Pilon, A novel external reflecting raceway pond design for improved biomass productivity, Algal Res. 65 (2022) 102742.
[35] Recommended practice for the calculation of daylight availability, J. Illum. Eng. Soc. 13 (4) (1984) 381–392, Publisher: Taylor & Francis _eprint: https://doi.org/10.1080/00994480.1984.10748791.
[36] Code of Federal Regulations, in: Occupational Health and Environmental Controls, Safety and Health Regulations for Construction no., 2024.
[37] J. Degen, A. Uebele, A. Retze, U. Schmid-Staiger, W. Trösch, A novel airlift photobioreactor with baffles for improved light utilization through the flashing light effect, J. Biotechnol. 92 (2) (2001) 89–94.
[38] J.U. Grobbelaar, Mass production of microalgae at optimal photosynthetic rates, in: Photosynthesis, IntechOpen, 2013.
[39] B. Baránková, D. Lazár, J. Nauš, A. Solovchenko, O. Gorelova, O. Baulina, G. Huber, L. Nedbal, Light absorption and scattering by high light-tolerant, fast-growing Chlorella vulgaris IPPAS C-1 cells, Algal Res. 49 (2020) 101881.
[40] R. Kandilian, A. Soulies, J. Pruvost, B. Rousseau, J. Legrand, L. Pilon, Simple method for measuring the spectral absorption cross-section of microalgae, Chem. Eng. Sci. 146 (2016) 357–368.
[41] J.J. Cullen, M.R. Lewis, The kinetics of algal photoadaptation in the context of vertical mixing, J. Plankton Res. 10 (5) (1988) 1039–1063.
[42] T. de Mooij, Z.R. Nejad, L. van Buren, R.H. Wijffels, M. Janssen, Effect of photoacclimation on microalgae mass culture productivity, Algal Res. 22 (2017) 56–67.
[43] J.P. Cañavate, L.M. Lubian, Tolerance of six marine microalgae to the cryoprotectants dimethyl sulfoxide and Methanol1, J. Phycol. 30 (3) (1994) 559–565, _eprint: https://onlinelibrary.wiley.com/doi/pdf/10.1111/j.0022-3646.1994.00559.x.
[44] C. Sorokin, R.W. Krauss, Effects of temperature & illuminance on chlorella growth uncoupled from cell division, Plant Physiol. 37 (1) (1962) 37–42.
[45] O. Bernard, B. Rémond, Validation of a simple model accounting for light and temperature effect on microalgal growth, Bioresour. Technol. 123 (2012) 520–527.
[46] C. Vejrazka, M. Janssen, G. Benvenuti, M. Streefland, R.H. Wijffels, Photosynthetic efficiency and oxygen evolution of Chlamydomonas reinhardtii under continuous and flashing light, Appl. Microbiol. Biotechnol. 97 (4) (2013) 1523–1532.
[47] A. Kuhl, H. Lorenzen, Chapter 10 handling and culturing of chlorella, in: D.M. Prescott (Ed.), Methods in Cell Biology, vol. 1, Academic Press, 1964, pp. 159–187.
[48] J.U. Grobbelaar, L. Nedbal, V. Tichý, Influence of high frequency light/dark fluctuations on photosynthetic characteristics of microalgae photoacclimated to different light intensities and implications for mass algal cultivation, J. Appl. Phycol. 8 (4) (1996) 335–343.
[49] D.G.M. Beersma, S. Daan, R.A. Hut, Accuracy of circadian entrainment under fluctuating light conditions: Contributions of phase and period responses, J. Biol. Rhythms 14 (4) (1999) 320–329, Publisher: SAGE Publications Inc.
[50] I.M. Sobol, On the distribution of points in a cube and the approximate evaluation of integrals, USSR Comput. Math. Math. Phys. 7 (4) (1967) 86–112.
[51] M. Görs, R. Schumann, D. Hepperle, U. Karsten, Quality analysis of commercial Chlorella products used as dietary supplement in human nutrition, J. Appl. Phycol. 22 (3) (2010) 265–276.
[52] C. Camarena-Bernard, V. Pozzobon, Evolving perspectives on lutein production from microalgae - A focus on productivity and heterotrophic culture, Biotech. Adv. (2024) 108375.
[53] G.M. Sullivan, R. Feinn, Using effect size—or why the P value is not enough, J. Grad. Med. Educ. 4 (3) (2012) 279–282.
[54] D. Yang, J.E. Dalton, A unified approach to measuring the effect size between two groups using SAS, in: SAS Global Forum, Vol. 335, Citeseer, 2012, pp. 1–6.
[55] I.M. Sobol, Global sensitivity indices for nonlinear mathematical models and their Monte Carlo estimates, Math. Comput. Simulation 55 (1) (2001) 271–280.